



# CeO<sub>2</sub> quantum dots through assisted-sol–gel methods: Syntheses, physicochemical characterization, and antibacterial studies

P. R. Rekha Chandran<sup>1</sup> · S. S. Gauri<sup>1</sup> · M. J. Reshma<sup>1</sup> · J. Jiya<sup>2</sup> · R. V. Mangalaraja<sup>3,4</sup> · S. Anas<sup>1</sup>

Received: 30 May 2024 / Accepted: 18 July 2024  
© Qatar University and Springer Nature Switzerland AG 2024

## Abstract

This study aims to explore innovative approaches for synthesizing ultra-fine ceria nanoparticles by employing diverse assisted-sol–gel syntheses such as microwave, sonochemical, reflux, and heating methods and a comparative property assessment of the resultant nanoparticles. The physicochemical properties of the synthesized nanoparticles were analyzed including, crystallinity, crystallite size, bonding characteristics, reflectance, band gap, optical emission, nanoparticle size, morphology, and surface charge features. Highly crystalline, structurally pure, spherical-shaped, positively charged CeO<sub>2</sub> nanoparticles were obtained in all the synthesis methods. Among the four methods, notable outcomes were given by cerium dioxide (CeO<sub>2</sub>) nanoparticles synthesized via a microwave-assisted sol–gel method. These nanoparticles feature nanocrystalline structures with additional monodisperse quantum dot formations of size  $3 \pm 1.5$  nm, distinguished by a band gap of approximately 3.05 eV, BET surface area of 76 m<sup>2</sup>/g and a prominent blue emission band at around 464 nm. Antibacterial assays unveiled the remarkable inhibitory effects of microwave-synthesized CeO<sub>2</sub> nanoparticles against gram-negative bacteria, including *E. coli* and *P. aeruginosa*. In the quest for targeted antibacterial agents, this narrow-spectrum bactericidal activity highlights the potential of these nanoparticles as targeted antibacterial agents, offering promising avenues for combating infections caused by Gram-negative bacterial strains.

**Keywords** Cerium dioxide · Assisted-sol–gel synthesis · Microwave · Sonochemical · Reflux · Antibacterial

## 1 Introduction

Cerium dioxide nanoparticles are considered one of the most manufactured nanoparticles globally, with an estimated annual production of roughly 1000 tons [1]. In recent years ceria-based materials have a great deal of interest from both

scientific and commercial points of view (Kowsuki et al., 2023). Cerium oxide nanoparticles (CeO<sub>2</sub> NPs) have been widely employed in catalysis [2], gas sensors [3], solid oxide fuel cells [4], solar cells [5], high refractive index materials [6], UV blockers [7], polishing materials [8]. Besides, it has application in commercial three-way catalysts (TWCs) for the purification of motor exhaust gases, and it acts as an oxygen partial-pressure regulator, keeping the reductant/oxidant ratio in the exhaust close to the stoichiometric value [9]. One of the most important rare earth elements, cerium is the second element in the lanthanide series and has unique properties due to its low reduction potential and sudden oscillation between Ce<sup>+3</sup> and Ce<sup>+4</sup> oxidation states [10]. Furthermore, it has a face-centered cubic fluorite structure [11] with the unit cell containing four cerium and eight oxygen atoms [12].

There are several methods to synthesize CeO<sub>2</sub> NPs such as Hydrothermal [13], Solvothermal [14], Thermal hydrolysis [15], Precipitation [16], Flame spray methods [17], Thermal decomposition [18], Reversed micelles [19], Inverse microemulsion [20], Sonochemical [21], Pulsed laser ablation [22, 23], High energy ball milling [24], Electrochemical

✉ S. Anas  
anas@tkmcas.ac.in

<sup>1</sup> Department of Chemistry, T.K.M. College of Arts and Science, Research Centre, University of Kerala, Kollam, Kerala, India

<sup>2</sup> Division of Microbiology, Department of Bioscience, Rajagiri College of Social Science, Kochi, Kerala, India

<sup>3</sup> Facultad de Ingeniería y Ciencias, Universidad Adolfo Ibáñez, Diag. Las Torres 2640, Peñalolén, Región Metropolitana, 7941169 Santiago, Chile

<sup>4</sup> Instituto Universitario de Investigación y Desarrollo Tecnológico (IDT), Universidad Tecnológica Metropolitana (UTEM), Ignacio Valdivieso, 2409 San Joaquín, Santiago, Chile

synthesis [25], and so on. Sol–gel method [26–29] has received much attention for synthesizing metal oxide nanoparticles which involve the hydrolysis and subsequent polycondensation reaction of metal alkoxide precursors to form a sol and finally to a network-like structure called gel. However, the traditional sol–gel method has certain drawbacks, such as the need for expensive precursors, clustered and diffused particles, and amorphous end products. Generally, calcination is needed in most cases, resulting in nano to micron-sized aggregated particles. Being a simple, economical, and low-temperature modified form of this, the assisted sol–gel method involves the preparation of ultrafine nano-sized particles with high homogeneity, reliability, reproducibility, and controllability.

In addition to the industrial applications, CeO<sub>2</sub> nanoparticles emerged as a promising material having fascinating applications in the biomedical field as therapeutic agents [30] such as in the treatment of oxidative stress diseases [31], neuroprotection, Alzheimer's disease [32], bioscaffolding [33], rheumatoid arthritis [34], inflammatory bowel disease [35], chronic wounds, diabetics, retinitis [36], etc. Recent progress of ceria in nanomedicine helps in treating viral, genetic, and cancerous diseases [22, 23]. They show excellent antioxidant properties [37] at physiological pH values and have shown protection from reactive oxygen species [38] in several animal model systems. Gram-negative bacterial infections are becoming more and more common all over the world. Drug-resistant bacteria have simultaneously emerged as a result of overuse of traditional antibiotics, which are harder to treat. Thus, there is an urgent need for novel, efficient therapeutic approaches with little potential to generate drug-resistant bacteria.

So, in the present study, we have attempted to prepare ultra-fine ceria nanoparticles through novel two-tier sol–gel-based synthesis methods, namely assisted-sol–gel methods. By carefully manipulating the reaction conditions and parameters, we have successfully synthesized four different cerium dioxide nanoparticles using distinct assisted-sol–gel methods, including microwave, sonochemical, reflux, and conventional heating methods. The samples synthesized were characterized using an X-ray Diffractometer (XRD), Fourier Transform Infrared Spectrometer (FTIR), UV–Vis. Diffused Reflectance Spectroscopy (DRS), Dynamic Light Scattering Analyser (DLS), Surface area analyzer (BET), Transmission Electron Microscope (TEM), Scanning Electron Microscope (SEM), and Photoluminescence Spectrophotometer (PL). After assessing the physicochemical properties of the samples using crystallographic, spectroscopic, and microscopic characterization tools, antibacterial studies of the prepared cerium dioxide nanoparticles were subsequently conducted. The prepared nanoparticles' efficacy against gram-positive and gram-negative bacteria was analyzed. The results obtained were compared and discussed

and a possible mechanism for the antibacterial activity is also presented.

## 2 Experimental

### 2.1 Materials

The Cerium nitrate hexahydrate (Ce(NO<sub>3</sub>)<sub>3</sub>·6H<sub>2</sub>O), Rankem Chemicals Ltd, 99%) was taken as the starting material for the preparation of CeO<sub>2</sub> nanoparticles. For the preparation of sol, 10% NH<sub>3</sub> (Nice, 99%), and 10% HNO<sub>3</sub> (Nice, 99%) were used. Double-distilled water was used for all the preparations.

### 2.2 Preparation of sol

A precise quantity of 2.1711 g (5 mM) Cerium nitrate hexahydrate (Ce(NO<sub>3</sub>)<sub>3</sub>·6H<sub>2</sub>O) was accurately weighed and dissolved in 1000 ml double-distilled water. The prepared solution was saturated with 10% NH<sub>3</sub> under stirring conditions until a Ce(OH)<sub>4</sub> precipitate was obtained. This was centrifuged and the precipitate was washed with warm double distilled water and centrifuged for 10 min at a speed of 3000 rpm. Then the residue was re-dissolved in 500 ml double distilled water. After the precipitate re-dissolving step, the pH of the solution was adjusted to the acidic range by adding 10% HNO<sub>3</sub> dropwise till a stable sol was obtained. A pH reading of 1.8 was finally obtained for the stable sol. The yellow sol was stirred for 1 h and then subjected to different assisted-sol–gel methods. The CeO<sub>2</sub> NPs synthesized from a 5 mM precursor solution of cerium nitrate were taken as the standard for all the characterization studies.

### 2.3 Synthesis of cerium oxide nanoparticles by assisted-sol–gel methods

The conditions adopted for the nanoceria synthesis by different assisted-sol–gel methods are summarized in Table 1. A schematic diagram showing the step-by-step process involved is provided in Fig. 1 and Fig. S1. The synthesis of cerium dioxide nanoparticles was carried out by treating the sol under different experimental conditions

**Table 1** Method of preparation and synthesis conditions for preparing Cerium Oxide nanoparticles by assisted-sol–gel methods

Sample Code	Method of Preparation	Conditions
Sample 1 (MS)	Microwave	1200W, 30Min
Sample 2 (SS)	Sonochemical	40 kHz, 1Hr
Sample 3 (RS)	Reflux	100 °C, 1Hr
Sample 4 (CS)	Conventional Heating	300 °C, 8Hrs

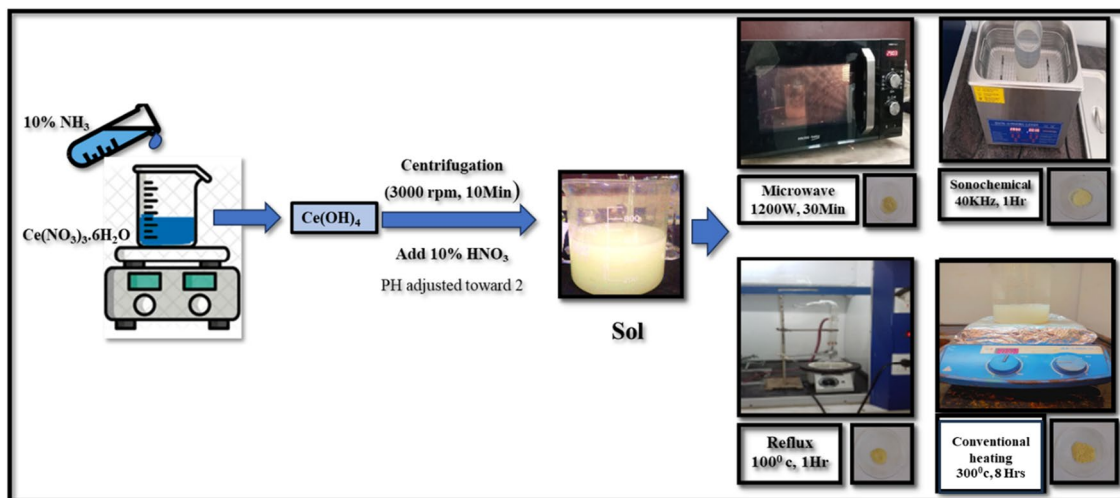


Fig. 1 Schematic diagram for the synthesis of cerium dioxide nanoparticles

comprising of, refluxing the sol at 100 °C for 1 h, ultrasonicated sol for 1 h at 40 kHz, microwave irradiation of sol at 1200 W for 30 min in a kitchen microwave, and conventional heating of the sol in a hot plate at 300 °C, 8Hrs. As detailed in Fig. 1, yellow-colored cerium oxide nanoparticles were finally obtained.

## 2.4 Characterization of CeO<sub>2</sub> nanoparticles

The crystallinity of the synthesized yellow-colored Ceria nanoparticles was studied using an X-ray diffractometer (XRD Rigaku MiniFlex, Japan) using CuK $\alpha$  radiation. The X-ray diffraction data was collected over the 2 $\theta$  range 20–80° and the analysis was done at medium scan speed. Scherrer's equation was used to calculate the crystallite size. The specific surface area and porosity of ceria nanoparticles were calculated using XRD. FT-IR spectra were recorded in the range of 4000–400 cm<sup>-1</sup> via an FTIR spectrometer (Shimadzu IR Affinity, Japan). The UV–Vis. Diffused reflectance spectra of CeO<sub>2</sub> NPs were recorded between 200 and 800 nm with the help of a UV–Vis. Spectrophotometer (Shimadzu, Japan). Size distribution analysis was performed with a dynamic light scattering analyzer (DLS, Anton Paar, Lifesizer 500). The morphology and average size of the nanoparticles were analyzed using TEM (JEOL JEM 1200 EX II, Japan). The bulk morphologies were also studied using an SEM (JSM-5610, Japan). The surface area of the samples was analyzed using BET (micromeritics Tristar II). The Photoluminescence (PL) spectra of prepared CeO<sub>2</sub> nanoparticles are measured and recorded using a Photoluminescence spectrophotometer (Varian, Cary).

## 2.5 Antibacterial activity studies

The CeO<sub>2</sub> NPs obtained from different sol-assisted methods were subjected to the present study. Antibacterial studies were performed by the disc diffusion method. The bacterial strains were purchased from the Cashew Export Promotion Council of India (CEPCI). A 10 ml suspension of nanoparticles (4 g/L) was sonicated and filtered. It was kept at room temperature in a desiccator. Using a sterile L-shaped glass rod, the bacterial suspension (*E. coli*, *P. aeruginosa*, *S. pyogenes*, *S. aureus*) was evenly applied to the surface of a nutrient agar plate. The surface of each agar plate was covered with filter paper soaked in nanoceria. Antibiotic (Amoxicillin) laden disks were placed on the nutrient agar plate. The plates were incubated at 35 °C for 24 h. The diameter of the inhibition zone was measured after the incubation period. To determine antibacterial activity, each sample was tested in triplicate, and the average values were computed.

## 3 Results and discussion

### 3.1 X-ray diffraction

The X-ray diffractograms of CeO<sub>2</sub> nanoparticles synthesized through different assisted sol–gel methods were provided in Fig. 2. The crystallographic studies revealed that all the diffractograms match well with the International Centre of Diffraction Data (ICDD) peaks of pure CeO<sub>2</sub> nanocrystals. Notably, the diffraction peaks were sharp, corresponding to the crystal planes (111), (200), (220), and (311) at 2 $\theta$  values 28°, 33°, 47° and 56°, respectively. This indicates the highly crystalline nature of the samples with a cubic fluorite structure. The

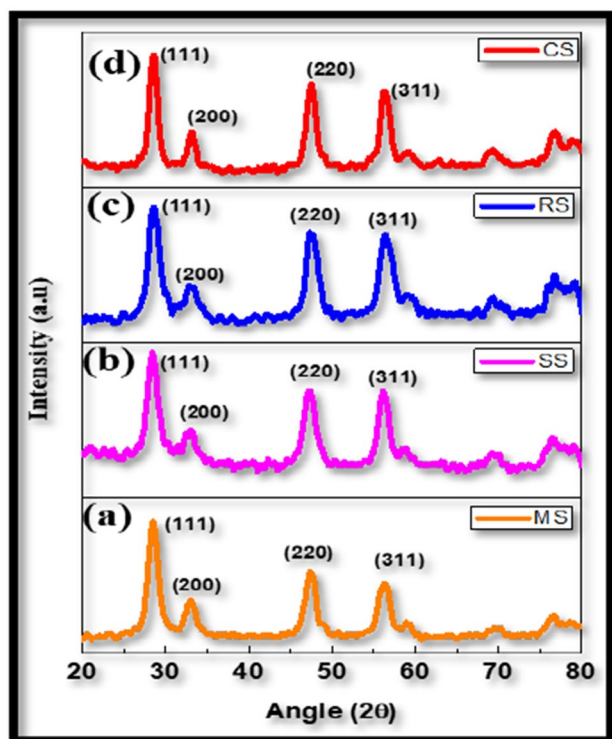


**Fig. 2** Powder X-ray diffraction patterns of CeO<sub>2</sub> NPs prepared from 5 mM cerium nitrate precursor solution using different assisted sol-gel methods (a) Microwave (b) Sonochemical (c) Reflux (d) Conventional heating

broadness of the diffraction peaks affirms the nano-size regime of the prepared CeO<sub>2</sub> particles. From the diffraction analyses, the average crystallite size *D* of the samples was calculated, using the Debye–Scherrer's formula [39],

$$D = k\lambda / \beta \cos\theta$$

where,  $k=0.94$ , called Scherer's constant, ' $\lambda$ ' is the wavelength of the X-ray used (1.5405 Angstrom), ' $\beta$ ' is the angular peak width at half maximum in radians, and ' $\theta$ ' is the diffraction angle. The diffraction studies confirmed that nanocrystalline cerium oxide nanoparticles were formed across all assisted sol-gel synthesis methods, with sizes falling within 5.01–5.82 nm. The average crystallite size of the prepared particles was, MS=5.34, SS=5.82, RS=5.38, and CS=5.01 nm, respectively. The specific surface area and porosity of ceria nanoparticles from XRD data were determined (Table S1). The specific surface area calculated from XRD data was also compared with the surface area measured using a BET analyzer (Table S2).

### 3.2 Fourier transform infrared spectroscopy

The FTIR spectra of the synthesized CeO<sub>2</sub> NPs were taken and provided in Fig. 3. All the samples showed three intense peaks in three ranges at 450–413 cm<sup>-1</sup>, 2380–2300,

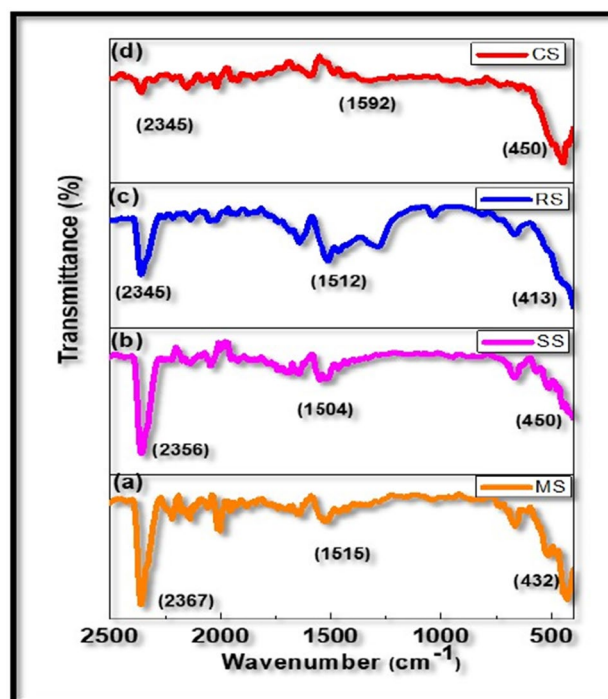


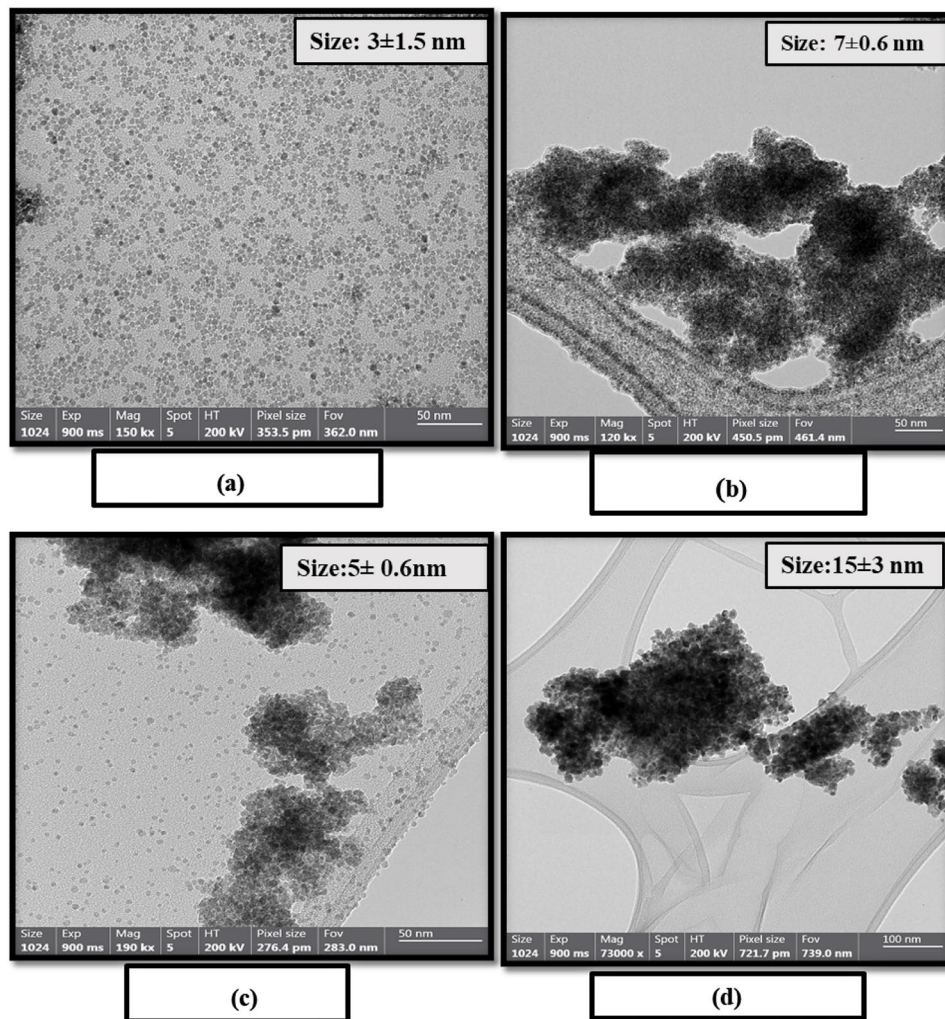
**Fig. 3** FTIR spectra of CeO<sub>2</sub> nanoparticles prepared from cerium nitrate by different assisted sol-gel methods (a) Microwave (b) Sonochemical (c) Reflux (d) Conventional

and 1592–1504. The intense band at 450–413 cm<sup>-1</sup> corresponds to the Ce–O stretching vibration. From the analysis, the absorption peak at around 1592–1504 cm<sup>-1</sup> is ascribed to the bending vibration of C–H units. The bands located at around 2380–2300 cm<sup>-1</sup> can be attributed to the CO<sub>2</sub> asymmetric stretching vibration and C–O stretching vibration [40]. The FTIR analyses further affirm the presence and formation of cerium oxide nanoparticles through various synthesis methods.

### 3.3 Transmission electron microscopy (TEM)

The morphology and particle size of the prepared samples were analyzed using transmission electron microscopy (TEM). Figure 4(a–d) displays TEM micrographs of four different nanoceria samples. Notably, all the employed techniques displayed spherical CeO<sub>2</sub> nanoparticles, but with varying size regimes. The samples exhibited a narrow size distribution. The particle size, as measured using ImageJ software, for samples MS, SS, RS, and CS were  $3 \pm 1.5$  nm,  $7 \pm 0.6$  nm,  $5 \pm 0.6$  nm, and  $15 \pm 3$  nm, respectively. Only the MS sample displayed monodisperse quantum dot-sized particles, while other samples SS, RS, and CS showed fine aggregated particles. This observation is further supported by the FESEM images (Fig. S2).

**Fig. 4** TEM images of ceria nanoparticles obtained by (a) microwave (MS), (b) sonochemical (SS), (c) reflux (RS), and (d) conventional (CS) heating-assisted sol–gel methods. Insets are the size range of the nanoparticles



### 3.4 Diffuse reflectance spectra and bandgap measurement

The diffuse reflectance spectra of the prepared CeO<sub>2</sub> NPs by different assisted sol–gel methods are provided in Fig. S3. The reflectance data was used for processing the band gap energy of the samples using the Tauc model equation [41],

$$(\alpha h\nu)^\gamma = A (h\nu - E_g)$$

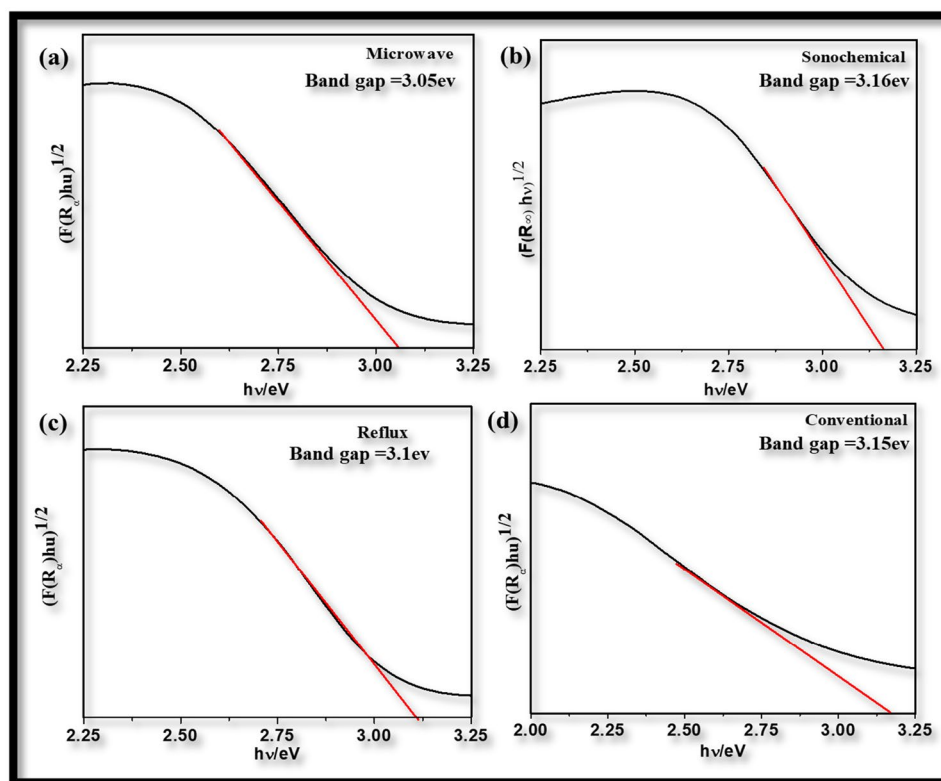
where ‘ $\alpha$ ’ is the absorption coefficient, ‘ $h$ ’ is the plank’s constant, ‘ $\nu$ ’ is the photon’s frequency, ‘ $A$ ’ is a proportionality constant, ‘ $E_g$ ’ is the band gap energy, and ‘ $\gamma$ ’ denotes the nature of the electronic transition. The value of ‘ $\gamma$ ’ is taken as ‘2’ for direct allowed transitions and as ‘1/2’ for indirect allowed transitions. The bandgap values were estimated by plotting  $(\alpha h\nu)^2$  on the Y-axis and the energy of the photon on the X-axis, the intercept of the straight line in the X-axis provided the bandgap value. Based on the Tauc plot analysis, as shown in Fig. 5, the optical band gap energies

of ceria nanoparticles synthesized using microwave, reflux, sonochemical, and conventional heating-assisted sol–gel methods were determined to be 3.05 eV, 3.10 eV, 3.16 eV, and 3.15 eV, respectively. Among all the synthesis methods, microwave-assisted sol–gel synthesis exhibited the smallest band gap energy when compared to other samples.

### 3.5 Photoluminescence

A photoluminescence spectrophotometer is used to explore the optical properties of prepared samples. Figure 6. depicts the photoluminescence spectra of ceria nanoparticles prepared through different assisted sol–gel methods. The spectra show a prominent and broad emission peak in the visible region, accompanied by minor secondary peaks. Especially, a distinct band appears consistently around 464 nm across all samples, indicative of the characteristic luminescence of CeO<sub>2</sub> nanoparticles. The analysis revealed that the emission band for CeO<sub>2</sub> samples ranging from 400–500 nm is related to doping from different defect levels of the range Cerium

**Fig. 5**  $[F(R_{\infty})h\nu]^{1/2}$  versus  $h\nu/eV$  plots of  $\text{CeO}_2$  nanoparticles obtained through (a) Microwave (MS), (b) Sonochemical (SS), (c) Reflux (RS), and (d) Conventional methods (CS)



4f to Oxygen 2p band [42]. The low-intensity green emission band may be due to the low-density oxygen vacancies present in the  $\text{CeO}_2$  NPs. The visible emission is induced by the radiative recombination of a photogenerated hole and an electron that fills the oxygen vacancy.

### 3.6 Zeta potential measurements

The zeta potential of the nanoparticles was meticulously assessed using a zeta potential analyzer and the corresponding plots are provided in Fig. 7. Remarkably, all samples exhibited a positive charge, emphasizing the robustness of the synthesis methods employed. Table 2 provides information about the zeta potential values and electrophoretic mobility of the prepared nanoparticles. The zeta potential values and electrophoretic mobility for ceria nanoparticles from different sol-assisted methods followed the order: Conventional > Sonochemical > Microwave > Reflux.

Of particular interest, the highest zeta potential value of +47.71 mV was observed for the ceria nanoparticles synthesized via the conventional heating-assisted sol–gel method, followed by +47.43 mV for sonochemical and +45.09 mV for microwave samples. This high zeta potential value signifies the exceptional stability of nanoparticles in a medium, attributed to the heightened

electrostatic repulsion that exists between the nanoparticles. This may further indicate the reduced aggregation and minimal agglomeration of nanoparticles. In contrast, the lowest zeta potential (+10.7 mV) was recorded for ceria nanoparticles obtained through the reflux-assisted sol–gel method. This lower value suggests the possibility of eventual aggregation due to Van der Waals inter-particle attractions [43].

### 3.7 Antibacterial studies

The antibacterial properties of the prepared Ceria nanoparticles from different assisted-sol–gel methods were evaluated against certain gram-positive and gram-negative bacteria. Notably, gram-negative bacteria such as *Escherichia coli* and *Pseudomonas aeruginosa*, alongside gram-positive counterparts *Streptococcus aureus* and *Streptococcus pyogenes*, were scrutinized. The photographic images of the antibacterial studies performed using  $\text{CeO}_2$  NPs prepared using different assisted sol–gel methods against *E. coli*, *P. aeruginosa*, *S. pyogenes*, and *S. aureus* bacteria are presented in Fig. 8. A comparative property evaluation of  $\text{CeO}_2$  nanoparticles synthesized using different assisted sol–gel methods is also provided in Table 3.

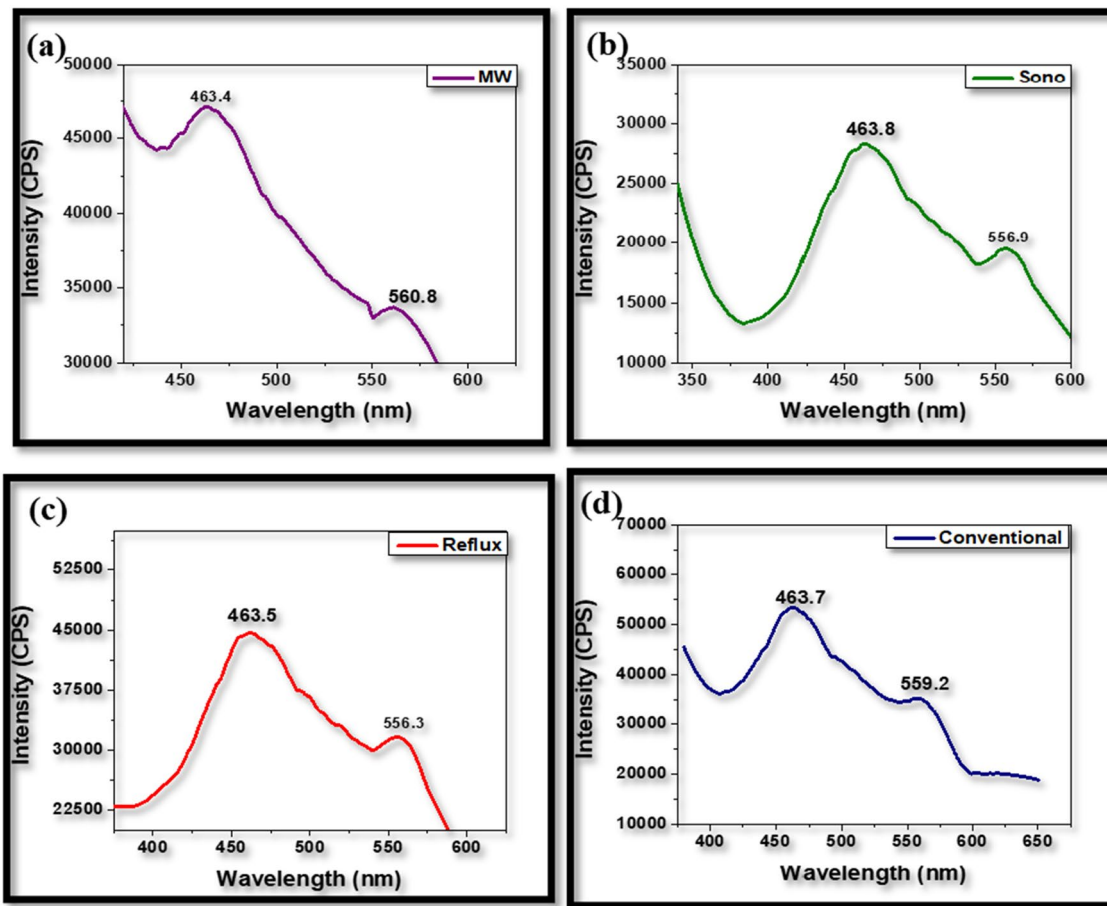


**Fig. 6** PL spectra of CeO<sub>2</sub> nanoparticles synthesized through (a) Microwave (MS), (b) sonochemical (SS), (c) reflux, and (d) conventional (CS) methods

The antibacterial studies indicate that the CeO<sub>2</sub> NPs synthesized through different assisted sol-gel methods do not exert any inhibitory effects on *S. pyogenes* and *S. aureus*, contrary to microwave-synthesized counterparts, which effectively inhibit *E. coli* and *Pseudomonas aeruginosa*. The inhibition Zone against different types of bacteria is mentioned in Table S3. The diameter of the inhibition zone (DIZ) indicates the magnitude of susceptibility of the microorganism. DIZ was measured on agar plates using a ruler with a 1 mm resolution and Image J Software (Fig S4). None of the prepared samples exhibited antibacterial activity against Gram-positive bacteria. This is attributed to Gram-positive bacteria's robust and dense cell walls, comprising thick layers of peptidoglycan and phosphoric acid (20–80 nm), rendering them more resilient to the antimicrobial effects of positively charged CeO<sub>2</sub> nanoparticles [44–47]. In contrast, the CeO<sub>2</sub> NPs obtained by the microwave-assisted method exhibited

a maximum of 18 mm and 16 mm DIZ against Gram-negative bacteria, *E. coli*, and *P. aeruginosa*, respectively. This specific activity can be attributed to the synergistic interplay between the factors affected. Firstly, Gram-negative bacteria are surrounded by a thin (< 10 nm) peptidoglycan cell wall, which is surrounded by an outer membrane containing anionic lipopolysaccharide which makes their surface more negative charge [48]. This facilitates strong electrostatic attraction between positively charged CeO<sub>2</sub> NPs and bacterial outer membranes, ultimately leading to bacterial cell death. Secondly, when compared to the other synthesizing methods, the CeO<sub>2</sub> nanoparticles synthesized through the microwave-assisted method have the least particle size and larger surface-to-volume ratio. This provides more active sites and a greater ability to inhibit the growth of bacteria, resulting in the spontaneous production of reactive oxygen species. Thus, MW-synthesized nanoparticles exhibited stronger

**Fig. 7** Zeta potential distribution curves of ceria nanoparticles obtained by (a) microwave (MS), (b) sonochemical (SS), (c) reflux, and (d) conventional (CS) methods

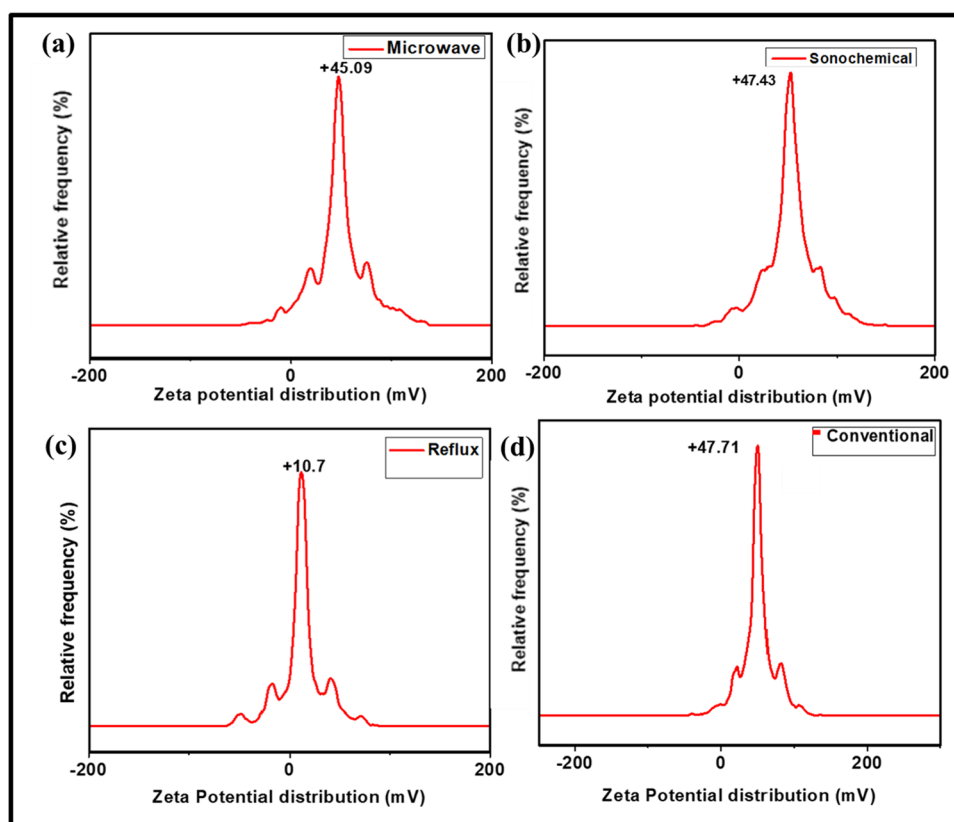


**Table 2** Zeta potential and electrophoretic mobility values of ceria nanoparticles prepared by (a) Microwave (MS), (b) Sonochemical (SS), (c) Reflux (RS), and (d) Conventional heating (CS) methods

Sl. No: Sample Code	Zeta Potential (mV)	Electrophoretic mobility
1. Microwave (MS)	+ 45.09	3.5555
2. Sonochemical (SS)	+ 47.43	3.6971
3. Reflux (RS)	+ 10.7	0.8361
4. Conventional (CS)	+ 47.71	3.7189

antimicrobial activity than other synthesized nanoparticles. The microwave-synthesized CeO<sub>2</sub> NPs exhibited a switchable antibacterial property, highlighting its potential for tailored antibacterial interventions.

It is also clear from Table 3 that, microwave and reflux-assisted synthesized CeO<sub>2</sub> nanoparticles have comparable particle sizes. However, the Zeta potential analysis revealed that the CeO<sub>2</sub> nanoparticles obtained from the reflux method showed the property of agglomeration (Fig. 7). This aggregation phenomenon may reduce their effectiveness in combating Gram-positive bacteria. Regarding ROS generation,

CeO<sub>2</sub> NPs act as a semiconductor with a bandgap falling in the 3.05–3.15 eV range. When it is exposed to light having energy greater than or equal to its bandgap energy, it will absorb the photons, and an electron–hole pair is formed by exciting an electron from filled VB to empty CB. These electrons and holes react with oxygen and water to form superoxide radicals and hydroxyl radicals respectively. The expected bactericidal mechanism is shown in Fig. 9. It is expected that the reactive oxygen species (ROS) penetrates the bacterial cell wall causing damage to the membrane releasing an abundant amount of cytosol from the cell and effective cell death. Gram-negative bacteria are generally more susceptible to mechanical lysis and osmotic rupture than gram-positive cells due to their peptidoglycan cell wall being thinner than those of gram-positive bacteria [49–51].

Thus, the antibacterial investigations from the present study affirm that ultra-fine CeO<sub>2</sub> nanoparticles can be treated as a narrow-spectrum antibiotic against gram-negative bacteria. This study shows that ultra-fine CeO<sub>2</sub> nanoparticles from microwave methods are viable candidates for a biocidal impact, which shows superior antibacterial activity on Gram-negative bacteria making them act as excellent antibacterial agents in the elimination of numerous harmful pathogens.



**Fig. 8** Representative images of agar plates containing CeO<sub>2</sub> nanoparticle-impregnated disks in *E. coli*, *P. aeruginosa*, *S. pyogenes*, and *S. aureus* bacteria

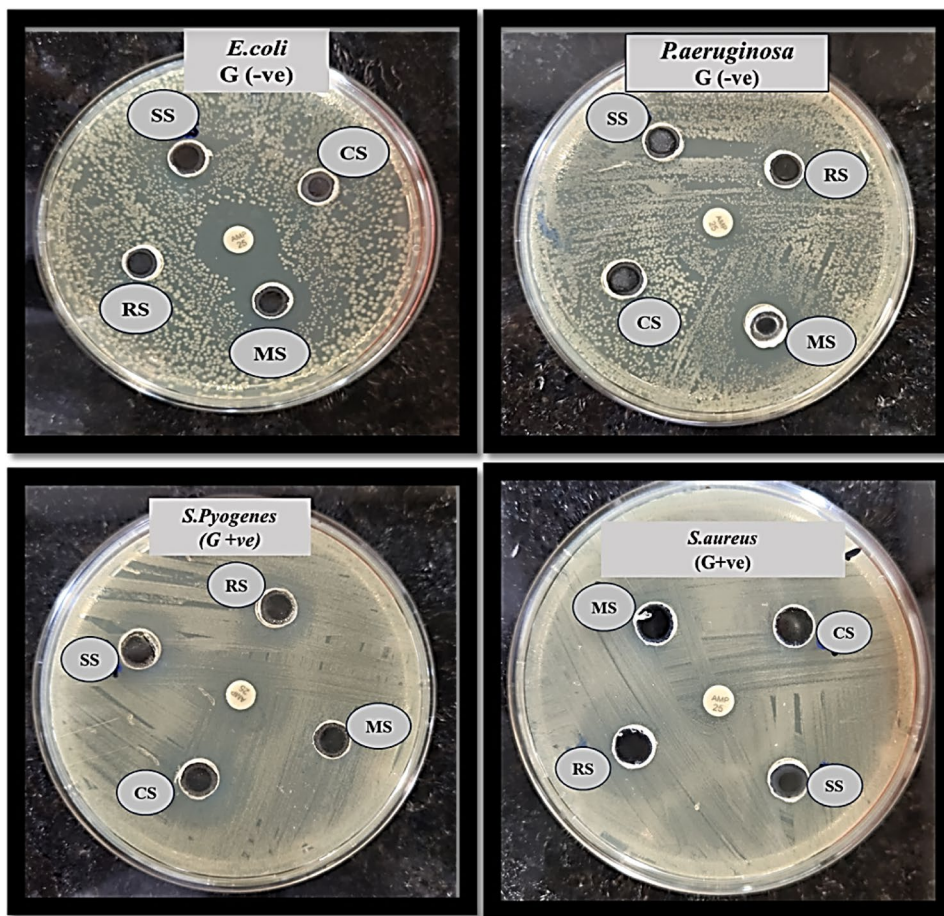
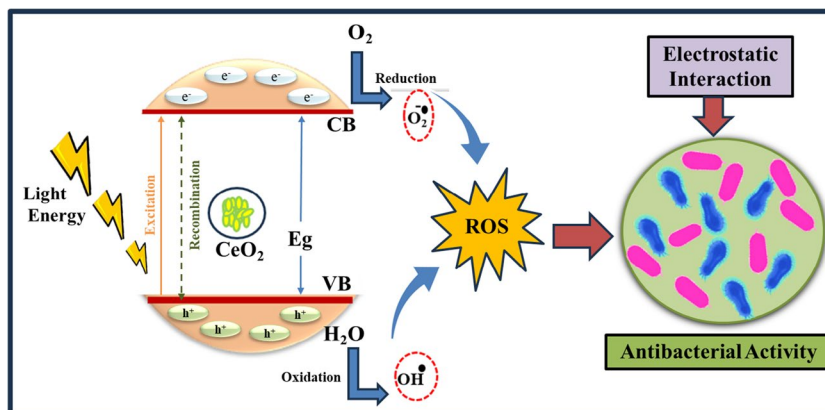


**Table 3** Comparative property analysis of CeO<sub>2</sub> nanoparticles synthesized using assisted-sol-gel methods

Sl No	Sample	Crystallite Size (nm)	Particle Size (nm)	Band Gap (eV)	Zeta Potential	Escherichia coli G (-ve)	Pseudomonas aeruginosa G (-ve)
1	Microwave	5.34	3 ± 1.5	3.05	+45.09	18 mm	16 mm
2	Sonochemical	5.82	7 ± 0.6	3.16	+47.43	Nil	Nil
3	Reflux	5.38	5 ± 0.6	3.10	+10.7	Nil	Nil
4	Conventional	5.01	15 ± 3	3.15	+47.71	Nil	Nil

**Fig. 9** The ROS-mediated antibacterial property of CeO<sub>2</sub> nanoparticles synthesized by microwave-assisted sol-gel synthesis



## 4 Conclusions

The versatility of the assisted-sol-gel method is addressed in the present investigation through comparative property assessment studies of ultra-fine cerium dioxide nanoparticles derived from different assisted-sol-gel methods, namely microwave, sonochemical, reflux, and conventional heating. The comparative physicochemical property assessment revealed that all the assisted-sol-gel synthesized CeO<sub>2</sub> nanoparticles exhibited cubic fluorite structures with comparable crystallite sizes, ranging from 5.01–5.82 nm. An intense FTIR band at 450–413 cm<sup>-1</sup> corresponds to the Ce–O stretching vibration observed by all the samples. The samples displayed nanosphere morphologies and exhibited high specific surface area values. Among the spherically shaped particles, the microwave-synthesized CeO<sub>2</sub> nanoparticles exhibited unique monodisperse characteristics. Except for the sol-dried conventionally prepared sample, all other samples exhibited nanoparticles in the quantum dot size regime. The samples were identified as semiconductors with good reflectance properties and their band gap values ranged from 3.05 eV to 3.16 eV. A pronounced blue emission band around 464 nm was observed for all the samples which is significant for the ultra-fine CeO<sub>2</sub> nanoparticles. All the prepared CeO<sub>2</sub> nanoparticles exhibited positive charges with high electrophoretic mobility values. The antibacterial studies disclosed the remarkable inhibitory effects of CeO<sub>2</sub> nanoparticles synthesized via the microwave-assisted sol-gel method against gram-negative bacteria such as *E. coli* and *P. aeruginosa*, highlighting their specificity towards Gram-negative strains. The current study thus put forth a few novel assisted-sol-gel methods having remarkable physicochemical properties, offering exciting prospects for the development of next-generation antibacterial agents with narrow-spectrum bactericidal capabilities.

**Supplementary Information** The online version contains supplementary material available at <https://doi.org/10.1007/s42247-024-00807-w>.

**Acknowledgements** The authors gratefully acknowledge CSIR-UGC for providing a senior research fellowship, and the Department of Science and Technology (FIST-SR/FST/College-213/2014(C) for the financial and facility support. The authors are also thankful to Mr. Peer Mohamed Abdul Azeed (CSIR—National Institute for Interdisciplinary Science and Technology, Trivandrum) for helping with the characterization tools.

**Authors contribution** Rekha Chandran P R: Idea creation, Investigation, Writing – review & editing.

Gauri S.S: Methodology, Formal analysis, Writing – review & editing.

Reshma Mariyam Jacob: Conceptualization, Writing – review & editing.

Jiya Jose- Formal analysis, Characterization studies.

Mangalaraja R.V– Sample Analysis, Instruments Support.

S. Anas—Supervision, Fund acquisition, Writing- review and editing.

All authors critically evaluated the work for intellectual content and approved the final version.

**Data Availability** All data generated or analysed during this study are included in this article.

## Declarations

**Competing interest** The authors declare that they have no known competing financial interests or personal relationships that could have appeared to influence the work reported in this paper.

## References

1. S. Pansambal, R. Oza, S. Borgave et al., Bioengineered cerium oxide (CeO<sub>2</sub>) nanoparticles and their diverse applications: a review. *Appl. Nanosci.* **13**, 6067–6092 (2023). <https://doi.org/10.1007/s13204-022-02574-8>
2. E.I. Isaeva, Gur'ev NV, Boitsova TB, et al., Photochemical synthesis and catalytic properties of materials containing cerium(IV) oxide and gold nanoparticles. *Russ. J. Gen. Chem.* **92**, 1972–1982 (2022). <https://doi.org/10.1134/S1070363222100115>
3. B.S. Rohini, H. Nagabhushana, G.P. Darshan et al., Fabricated CeO<sub>2</sub> nanopowders as a novel sensing platform for advanced forensic, electrochemical, and photocatalytic applications. *Appl. Nanosci.* **7**, 815–833 (2017). <https://doi.org/10.1007/s13204-017-0611-x>
4. T.B. Ronaghi, F. Fotovat, S.A.H. Zamzajian, Enhancing cerium oxide nanoparticle stability in diesel-biodiesel blends via alumina nanoparticle amalgamation. *Waste. Biomass. Valor.* (2024). <https://doi.org/10.1007/s12649-024-02573-6>. Accessed 23 May 2024
5. M. Danish, H. Ayub, Z.A. Sandhu et al., Synthesis of cerium oxide/cadmium sulfide nanocomposites using inverse micro-emulsion methodology for photocatalytic degradation of methylene blue. *Appl. Nanosci.* **11**, 2503–2515 (2021). <https://doi.org/10.1007/s13204-021-02027-8>
6. D. Mal, A. Balouch, Sirajuddin, et al., Synthesis and catalytic practicality of CeO<sub>2</sub> nanoparticle: an excellent heterogenous candidate for 4-nitrophenol reduction. *Appl. Nanosci.* **10**, 3443–3455 (2020). <https://doi.org/10.1007/s13204-020-01472-1>
7. V. Gautham, C. Chinglenthoba, J. John, V. Sajith, Enhancement of soot combustion in diesel particulate filters by ceria nanofiber coating. *Appl. Nanosci.* **10**, 2429–2438 (2020). <https://doi.org/10.1007/s13204-020-01425-8>
8. X. Bi, C. Zeng, P. Westerhoff, Adsorption of Arsenic Ions Transforms Surface Reactivity of Engineered Cerium Oxide Nanoparticles. *Environ. Sci. Technol.* **54**, 9437–9444 (2020). <https://doi.org/10.1021/acs.est.0c02781>
9. N. Qadeer, N. Jabeen, L.U. Khan et al., Hydrothermal synthesis and characterization of transition metal (Mn/Fe/Cu) co-doped cerium oxide-based nano-additives for potential use in the reduction of exhaust emission from spark ignition engines. *RSC Adv.* **12**, 15564–15574 (2022). <https://doi.org/10.1039/D2RA01954J>
10. V. Seminko, P. Maksimchuk, G. Grygorova et al., Mechanism and dynamics of fast redox cycling in cerium oxide nanoparticles at high oxidant concentration. *J Phys Chem C* **125**, 4743 (2021). <https://doi.org/10.1021/acs.jpcc.1c00382>
11. K.R. Singh, V. Nayak, T. Sarkar, R.P. Singh, Cerium oxide nanoparticles: properties, biosynthesis and biomedical application. *RSC Adv.* **10**, 27194–27214 (2020). <https://doi.org/10.1039/D0RA04736H>
12. A. Miri, M. Sarani, M. Khatami, Nickel-doped cerium oxide nanoparticles: biosynthesis, cytotoxicity and UV protection

- studies. *RSC Adv.* **10**, 3967–3977 (2020). <https://doi.org/10.1039/C9RA09076B>
13. S. Moeen, M. Ikram, A. Haider et al., Comparative Study of Sonophotocatalytic, Photocatalytic, and Catalytic Activities of Magnesium and Chitosan-Doped Tin Oxide Quantum Dots. *ACS Omega* **7**, 46428–46439 (2022). <https://doi.org/10.1021/acsomega.2c05133>
  14. W. Hu, L. Yang, P. Shao et al., Proton self-enhanced hydroxyl-enriched cerium oxide for effective arsenic extraction from strongly acidic wastewater. *Environ. Sci. Technol.* **56**, 10412–10422 (2022). <https://doi.org/10.1021/acs.est.2c02675>
  15. E. Özkan, A. Hofmann, M. Votsmeier et al., Comprehensive Characterization of a Mesoporous Cerium Oxide Nanomaterial with High Surface Area and High Thermal Stability. *Langmuir* **37**, 2563–2574 (2021). <https://doi.org/10.1021/acs.langmuir.0c0274>
  16. J.M. Yong, L. Fu, F. Tang et al., ROS-mediated anti-angiogenic activity of cerium oxide nanoparticles in melanoma cells. *ACS Biomater. Sci. Eng.* **8**, 512–525 (2022). <https://doi.org/10.1021/acsbomaterials.1c01268>
  17. X. Chen, G. Zou, Y. Yuan et al., Flame spray pyrolysis synthesized Ni-doped Fe/Ce oxygen carriers for chemical looping dry reforming of methane. *Fuel* **343**, 127913 (2023). <https://doi.org/10.1016/j.fuel.2023.127913>
  18. N. Agasti, M.A. Astle, G.A. Rance et al., Cerium oxide nanoparticles inside carbon nanoreactors for selective allylic oxidation of cyclohexene. *Nano. Lett.* **20**, 1161–1171 (2020). <https://doi.org/10.1021/acs.nanolett.9b04579>
  19. Y. Wu, H.T. Ta, Different approaches to synthesizing cerium oxide nanoparticles and their corresponding physical characteristics, and ROS scavenging and anti-inflammatory capabilities. *J Mater Chem B* **9**, 7291–7301 (2021). <https://doi.org/10.1039/D1TB01091C>
  20. M.W. Iqbal, Y. Yu, D.S.A. Simakov, Enhancing the surface area stability of the cerium oxide reverse water gas shift nanocatalyst via reverse microemulsion synthesis. *Catal. Today* **407**, 230–243 (2023). <https://doi.org/10.1016/j.cattod.2021.11.029>
  21. K.B. Kusuma, M. Manju, C.R. Ravikumar et al., Photocatalytic degradation of Methylene Blue and electrochemical sensing of paracetamol using Cerium oxide nanoparticles synthesized via sonochemical route. *Appl Surf Sci Adv* **11**, 100304 (2022). <https://doi.org/10.1016/j.apsadv.2022.100304>
  22. W. Zhu, Y. Lin, L. Zhu et al., Synthesis of cerium dioxide nanoparticles by gas/liquid pulsed discharge plasma in a slug flow reactor. *ACS Omega* **6**, 20966–20974 (2021). <https://doi.org/10.1021/acsomega.1c02463>
  23. C. Zhu, Z. Ji, J. Ma et al., Recent advances of nanotechnology-facilitated bacteria-based drug and gene delivery systems for cancer treatment. *Pharmaceutics* **13**, 940 (2021). <https://doi.org/10.3390/pharmaceutics13070940>
  24. R. Kasuya, Z.L. Bujňáková, M. Baláž et al., Novel Mechanically Assisted Dissolution of Platinum Using Cerium(IV) Oxide. *ACS Sustainable Chem Eng* **10**, 15357–15364 (2022). <https://doi.org/10.1021/acssuschemeng.2c01470>
  25. A. Karimi, S. Andreescu, D. Andreescu, Single-particle investigation of environmental redox processes of arsenic on cerium oxide nanoparticles by collision electrochemistry. *ACS Appl. Mater. Interfaces* **11**, 24725–24734 (2019). <https://doi.org/10.1021/acsami.9b05234>
  26. Anas, S., Mahesh, K.V., Jeen, M et al., Sol-Gel Materials for Varistor Devices. *Sol-Gel Materials for Energy, Environment and Electronic Applications* (eds). Springer 23–59. (2017). [https://link.springer.com/chapter/https://doi.org/10.1007/978-3-319-50144-4\\_2](https://link.springer.com/chapter/https://doi.org/10.1007/978-3-319-50144-4_2).
  27. S. Anas, P. Mukundan, A.M. Sanoj et al., Synthesis of ZnO-based nanopowders via a non-hydrolytic sol-gel technique and their densification behaviour and varistor properties. *Process Appl Ceram* **4**, 7–14 (2010)
  28. A.S. Fudala, W.M. Salih, F.F. Alkazzaz, Synthesis of different sizes of cerium oxide CeO<sub>2</sub> nanoparticles by using different concentrations of precursor via sol–gel method. *Mater Today Proc* **49**, 2786–2792 (2022). <https://doi.org/10.1016/j.matpr.2021.09.452>
  29. M.J. Reshma, J. Jiya, M. Anshida et al., A two-tier synthetic marvel for developing antibacterial, self-cleaning, durable, transparent, and superhydrophobic surfaces using zinc oxide - methyltrimethoxysilane hybrids. *J. Environ. Chem. Eng.* **12**, 112007 (2024). <https://doi.org/10.1016/j.jece.2024.112007>
  30. F. Asgharzadeh, A. Hashemzadeh, F. Rahmani et al., Cerium oxide nanoparticles act as a novel therapeutic agent for ulcerative colitis through anti-oxidative mechanism. *Life Sci.* **278**, 119500 (2021). <https://doi.org/10.1016/j.lfs.2021.119500>
  31. C.S. Shin, R.A. Veetil, T.S. Sakthivel et al., Noninvasive Delivery of Self-Regenerating Cerium Oxide Nanoparticles to Modulate Oxidative Stress in the Retina. *ACS Appl. Bio Mater.* **5**, 5816–5825 (2022). <https://doi.org/10.1021/acsbam.2c00809>
  32. B. Rahimi, Z. Behroozi, A. Motamednezhad et al., Study of nerve cell regeneration on nanofibers containing cerium oxide nanoparticles in a spinal cord injury model in rats. *J. Mater. Sci. Mater. Med.* **34**, 9 (2023). <https://doi.org/10.1007/s10856-023-06711-9>
  33. S. Ren, Y. Zhou, K. Zheng et al., Cerium oxide nanoparticles loaded nanofibrous membranes promote bone regeneration for periodontal tissue engineering. *Bioact Mater* **7**, 242–253 (2022). <https://doi.org/10.1016/j.bioactmat.2021.05.037>
  34. Z. Li, X. Wu, W. Gu et al., Photogenerated electrons from CeO<sub>2</sub> via upconversion of excitons to conduction band enhanced photocatalysis for Photo-Therapy of Rheumatoid arthritis. *Chem. Eng. J.* **446**, 136904 (2022). <https://doi.org/10.1016/j.cej.2022.136904>
  35. Y. Gao, J. Zou, B. Chen et al., Hyaluronic acid/serotonin-decorated cerium dioxide nanomedicine for targeted treatment of ulcerative colitis. *Biomater Sci* **11**, 618–629 (2023). <https://doi.org/10.1039/D2BM01256A>
  36. M.A. Stager, J. Bardill, A. Richard et al., Photopolymerized Zwitterionic Hydrogels with a Sustained Delivery of Cerium Oxide Nanoparticle-miR146a Conjugate Accelerate Diabetic Wound Healing. *ACS Appl. Bio Mater.* **5**, 1092–1103 (2022). <https://doi.org/10.1021/acsbam.1c01155>
  37. K. Siposova, V. Huntosova, I. Garcarova et al., Dual-Functional Antioxidant and Anti-amyloid Cerium Oxide Nanoparticles Fabricated by Controlled Synthesis in Water-Alcohol Solutions. *Bio-medicines* **10**, 942 (2022). <https://doi.org/10.3390/biomedicines10050942>
  38. Y. Wang, Z. Tan, Z. Zhang et al., Facet-Dependent Activity of CeO<sub>2</sub> nanozymes regulate the fate of human neural progenitor cell via redox homeostasis. *ACS Appl. Mater. Interfaces* **14**, 35423–35433 (2022). <https://doi.org/10.1021/acsbam.2c0930>
  39. K.B. Babitha, V. Linsha, S. Anas et al., Microwave-assisted aqueous synthesis of organosilane treated mesoporous Si@ZnO nano architectures as dual-functional, photocatalysts. *J. Environ. Chem. Eng.* **3**, 1337–1345 (2015). <https://doi.org/10.1016/j.jece.2014.12.010>
  40. J. Amala, M.J. Reshma, B. Irfana et al., Facile tartaric acid assisted microwave synthesis of spherical clusters of S, N, and C Doped ZnO for solar photocatalytic applications. *Mater. Lett.* **324**, 132714 (2022). <https://doi.org/10.1016/j.matlet.2022.132714>
  41. Ananthakumar, S., Anas, S., Ambily, J. et al. Microwave-assisted citrate gel combustion synthesis of ZnO, Part-II: Assessment of functional properties. *J. Ceram. Process Res.* **10**:164–169. (2010). <http://ir.niist.res.in:8080/jspui/handle/123456789/1551>.
  42. G. Jayakumar, A. Albert Irudayaraj, A. Dhayal Raj et al., Electrical and magnetic properties of nanostructured Ni doped CeO<sub>2</sub> for optoelectronic applications. *J. Phys. Chem. Solids* **160**, 110369 (2022). <https://doi.org/10.1016/j.jpcs.2021.110369>

43. S. Shrestha, B. Wang, P. Dutta, Nanoparticle processing: Understanding and controlling aggregation. *Adv. Colloid Interface Sci.* **279**, 102162 (2020). <https://doi.org/10.1016/j.cis.2020.102162>
44. T. Gasti, V.D. Hiremani, S.S. Kesti et al., Physicochemical and Antibacterial Evaluation of Poly (Vinyl Alcohol)/Guar Gum/Silver Nanocomposite Films for Food Packaging Applications. *J. Polym. Environ.* **29**, 3347–3363 (2021). <https://doi.org/10.1007/s10924-021-02123-4>
45. K.C. Rahlwes, I.L. Sparks, Y.S. Morita, Cell Walls and Membranes of Actinobacteria. *Subcell. Biochem.* **92**, 417–469 (2019). <https://doi.org/10.1007/978-3-030-18768-213>
46. F. Shaheen, M. Imran, A. Haider et al., Size-controlled synthesis of La and chitosan doped cobalt selenide nanostructures for catalytic and antibacterial activity with molecular docking analysis. *Int. J. Biol. Macromol.* **263**, 130096 (2024). <https://doi.org/10.1016/j.ijbiomac.2024.130096>
47. V. Stanić, S.B. Tanasković, Chapter 11 - Antibacterial activity of metal oxide nanoparticles, in *Nanotoxicity*. ed. by S. Rajendran, A. Mukherjee, T.A. Nguyen et al. (Elsevier, 2020), pp.241–274
48. N.J. Bassous, C.B. Garcia, T.J. Webster, A Study of the Chemistries, Growth Mechanisms, and Antibacterial Properties of Cerium- and Yttrium-Containing Nanoparticles. *ACS Biomater. Sci. Eng.* **7**, 1787–1807 (2021). <https://doi.org/10.1021/acsbiomaterials.0c00776>
49. E. Karimi, Antimicrobial Activities of Nanoparticles, in *Nanotechnology for Agriculture: Crop Production & Protection*. ed. by D.G. Panpatte, Y.K. Jhala (Springer, Singapore, 2019), pp.171–206
50. J. Sun, S.T. Rutherford, T.J. Silhavy, K.C. Huang, Physical properties of the bacterial outer membrane. *Nat. Rev. Microbiol.* **20**, 236–248 (2022). <https://doi.org/10.1038/s41579-021-00638-0>
51. K. Kawasaki, R. Nirmala, Y.-H. Ra, R. Navamathavan, Recent advances in cerium oxide-based nanocomposites in synthesis, characterization, and energy storage applications: A comprehensive review. *Results Chem* **5**, 100877 (2023). <https://doi.org/10.1016/j.rechem.2023.100877>
52. S.N. Naidi, M.H. Harunsani, A.L. Tan, M.M. Khan, Green-synthesized CeO<sub>2</sub> nanoparticles for photocatalytic, antimicrobial, antioxidant and cytotoxicity activities. *J Mater Chem B* **9**, 5599–5620 (2021). <https://doi.org/10.1039/D1TB00248A>

Springer Nature or its licensor (e.g. a society or other partner) holds exclusive rights to this article under a publishing agreement with the author(s) or other rightsholder(s); author self-archiving of the accepted manuscript version of this article is solely governed by the terms of such publishing agreement and applicable law.